Creating cell-specific computational models of stem cell-derived cardiomyocytes using optical experiments

Janice Yang,[1] Neil Daily,[2] Taylor K. Pullinger,[1] Tetsuro Wakatsuki,[2] Eric A. Sobie[1,*]

[1]Department of Pharmacological Sciences & Graduate School of Biomedical Sciences, Icahn School of Medicine at Mount Sinai, New York, NY, USA

[2]InvivoSciences Inc., Madison, WI 53719, USA.

Short Title: Optimizing parameter identification algorithms

*Corresponding author: eric.sobie@mssm.edu

Aim: To generate predictive cell line-specific computational models of stem cell-derived cardiomyocytes

Focus: Optimizing a computational pipeline for parameterizing models

Abstract:

Human induced pluripotent stem cell-derived cardiomyocytes (iPSC-CMs) have gained traction as a powerful model in cardiac disease and therapeutics research, since iPSCs are self-renewing and can be derived from healthy and diseased patients without invasive surgery. However, current iPSC-CM differentiation methods produce cardiomyocytes with immature, fetal-like electrophysiological phenotypes, and the variety of maturation protocols in the literature results in phenotypic differences between labs. Heterogeneity of iPSC donor genetic backgrounds contributes to additional phenotypic variability. Several mathematical models of iPSC-CM electrophysiology have been developed to help understand the ionic underpinnings of, and to simulate, various cell responses, but these models individually do not capture the phenotypic variability observed in iPSC-CMs. Here, we tackle these limitations by developing a computational pipeline to calibrate cell preparation-specific iPSC-CM electrophysiological parameters.

We used the genetic algorithm (GA), a heuristic parameter calibration method, to tune ion channel parameters in a mathematical model of iPSC-CM physiology. To systematically optimize an experimental protocol that generates sufficient data for parameter calibration, we created simulated datasets by applying various protocols to a population of *in silico* cells with known conductance variations, and we fitted to those datasets. We found that calibrating models to voltage and calcium transient data under 3 varied experimental conditions, including electrical pacing combined with ion channel blockade and changing buffer ion concentrations, improved model parameter estimates and model predictions of unseen channel block responses. This observation held regardless of whether the fitted data were normalized, suggesting that normalized fluorescence recordings, which are more accessible and higher throughput than patch clamp recordings, could sufficiently inform conductance parameters. Therefore, this computational pipeline can be applied to different iPSC-CM preparations to determine cell line-specific ion channel properties and understand the mechanisms behind variability in perturbation responses.

Author Summary:

Many drug treatments or environmental factors can trigger cardiac arrhythmias, which are dangerous and often unpredictable. Human cardiomyocytes derived from donor stem cells have proven to be a promising model for studying these events, but variability in donor genetic background and cell maturation methods, as well as overall immaturity of stem cell-derived cardiomyocytes relative to the adult heart, have hindered reproducibility and reliability of these studies. Mathematical models of these cells can aid in understanding the underlying electrophysiological contributors to this variability, but determining these models' parameters for multiple cell preparations is challenging. In this study, we tackle these limitations by developing a computational method to simultaneously estimate multiple model parameters using data from imaging-based experiments, which can be easily scaled to rapidly characterize multiple cell lines. This method can generate many personalized models of individual cell preparations, improving drug response predictions and revealing specific differences in electrophysiological properties that contribute to variability in cardiac maturity and arrhythmia susceptibility.

ABBREVIATIONS

- **AP:** Action potential

- **CaT:** Calcium transient

- **GA:** Genetic algorithm

- **G_x, I_x, J_x:** Maximal conductance (G), current density (I), or flux (J) for x, where x can be: Na (Na^+), f (funny Na^+), CaL (L-type Ca^{2+}), to (transient outward K^+), Ks (slow delayed rectifier K^+), Kr (rapid delayed rectifier K^+), K1 (inward rectifier K^+), PMCA (plasma membrane Ca^{2+} ATPase), bNa (background Na^+), bCa (background Ca^{2+}), Up (SR Ca^{2+} uptake), rel (SR Ca^{2+} release), NCX (Na^+/Ca^{2+} exchanger), NaK (Na^+/K^+ ATPase), SRleak (SR leak), or CaT (T-type Ca^{2+})

- **iPSC-CM:** Induced pluripotent stem cell-derived cardiomyocyte

- **LTCC:** L-type calcium channel

- **NCX:** Sodium-calcium exchanger

- **SERCA:** Sarco/endoplasmic reticulum calcium ATPase

- **SR:** Sarcoplasmic reticulum

4

83 **GLOSSARY**

84 - **Model/parameter calibration**: tuning one or more parameters in the computational model so that the

85 model output more closely matches experimental data

86 - **Experiment/protocol optimization**: the process of determining what type and amount of data is

87 sufficient but also feasible for our model calibration goals

88 - Protocol conditions – buffer calcium, potassium, or sodium concentrations; addition or removal

89 of stimulus; pacing rates; channel block; etc.

90 - Protocol length(?) – number of protocol conditions

91 - Protocol data type(?) –AP, CaT, or both; normalized or non-normalized data

92 - **Model prediction**: using the calibrated computational model to simulate response to *new (unseen)*

93 conditions, drugs, or perturbations (in our case, I_{Kr} block)

94 - Papers on independent validation/prediction

95 **Computational pipeline**: the full process of iPSC-CM computational model calibration; Includes iPSC-CM

96 data acquisition/simulation -> data processing -> parameter calibration using genetic algorithm -> validation of

97 calibrated models on an unseen condition (i.e. evaluating model predictions)

98

INTRODUCTION

99

100 Human iPSC-derived cardiomyocytes (iPSC-CMs) are derived from patient cells that have been reprogrammed

101 into pluripotency and subsequently manipulated to differentiate into the cardiac cell lineage. The development

102 of this *in vitro* platform marked a technological breakthrough in cardiac research, and iPSC-CMs are now

103 widely-used in cardiac pharmacology and disease research. iPSCs can be sourced through minimally-invasive

104 procedures, such as skin biopsy or blood draw, and maintained or banked for long periods [1,2]. These

105 properties of iPSC-CMs make them an ideal platform for pharmacological studies and personalized disease

106 modeling [3]. However, electrophysiological variability between iPSC-CM preparations from different cell lines

107 and differentiation methods limit the potential of this platform [4,5].

108 Mathematical models of cardiomyocyte electrophysiology can provide valuable insight into iPSC-CM

109 electrophysiological variability. These models contain parameters describing the ionic currents and fluxes that

110 contribute to the properties of cardiac action potential (AP) and calcium transient (CaT) waveforms. Several

111 models of iPSC-CM physiology exist in the literature [6–8], with the most recent and comprehensive model

112 published by Kernik et al. in 2019, hereon referred to as the "Kernik model" [9]. However, the baseline

113 parameter values in these models are not representative of the electrophysiological heterogeneity observed in

114 iPSC-CMs. Additionally, parameter calibration has often relied on separate patch clamp measurements of each

115 type of current. This process is time-consuming, inaccessible to many research groups, and often captures the

116 physiology of only the average behavior of the population of cells examined. Methods to simultaneously

117 optimize several or all model parameters using minimal data are under development [10–14]. Recent work on

118 guinea pig ventricular myocyte models [13] and human iPSC-CM models [14] have demonstrated the utility of

119 automated tuning algorithms for improving model parameterization. For example, in Devenyi et al [13], an

120 adjusted model, constrained by data, predicted the effect of slow delayed rectifier K^+ current (I_{Ks}) block more

121 accurately compared to baseline model. Analogous work, at the level of individual ion channels, has shown the

122 superiority of sinusoidal voltage clamp protocols, compared with traditional square-wave protocols, for

123 calibration of channel kinetic parameters [15].

124 Even with recent advances in iPSC-CM maturation protocols [16–19], most iPSC-CMs still display embryonic-

125 or neonatal-like cardiac phenotypes with different AP and CaT shapes compared with adult myocytes. These

6

126 phenotypic differences, and how they change temporally, can depend on subtle differences in cell culture

127 conditions and the genetic background of the cell donor [4,5,20], which likely contributes to the wide variation

128 observed between studies [4,5]. No standardized procedure currently exists for characterizing iPSC-CM

129 heterogeneity; prior efforts have generally examined a handful of molecular markers [21], used subjective

130 observations of physiology [22,23], or employed specialized methods such as single cell RNA sequencing

131 [24,25]. These factors, and the potential importance of iPSC-CMs as a research platform, highlight the need for

132 automated methods to characterize the cell lines used in each study.

133 Here we combined these ideas of simultaneous calibration of multiple parameters and optimization of a

134 minimal experimental protocol for generating calibration data. We aimed to create digital twins of iPSC-CM cell

135 preparations from the Kernik iPSC-CM model, thereby connecting observed iPSC-CM electrophysiology with

136 molecular function and mechanisms. We hypothesize that fluorescence readouts of iPSC-CM physiology under

137 varied experimental conditions provide enough information to reveal cellular ion channel properties, which can

138 then be incorporated into the iPSC-CM digital twins. To systematically evaluate various data types and

139 experimental protocols in their ability to inform model parameters, we created a simulated, *in silico* dataset

140 from Kernik model variations with known parameter values. From this study, we developed a computational

141 pipeline which includes: 1) an optimized protocol for fluorescence recordings of iPSC-CM preparations; 2) a

142 genetic algorithm process for calibration of ion channel parameters in iPSC-CM computational model, using

143 the experimental recordings; and 3) validation of the resulting calibrated models by evaluating their predictions

144 on independent, yet physiologically-important, perturbations. We demonstrate the utility of our computational

145 pipeline in generating iPSC-CM digital twins that capture ionic variability and predict cell-specific

146 electrophysiological phenotypes, including drug-induced arrhythmia susceptibility.
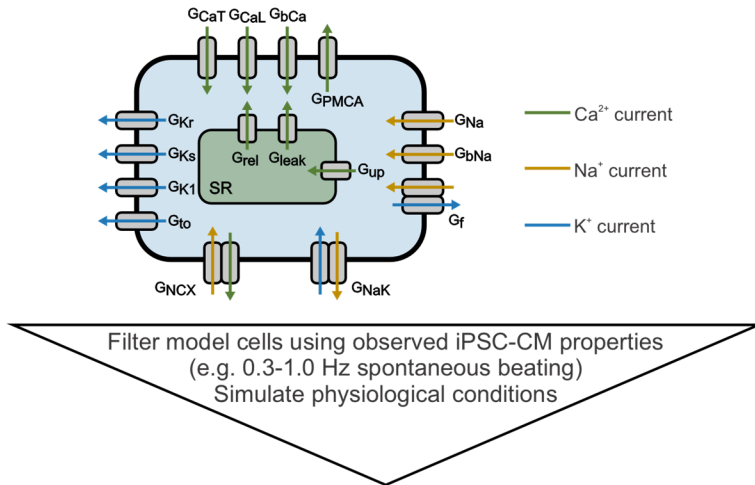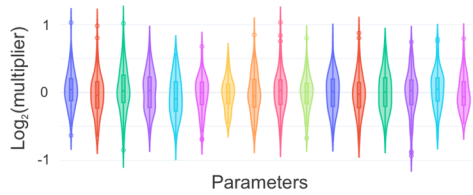
147 **RESULTS**

148   Our primary objective was to optimize an experimental protocol for generating sufficient data to calibrate an

149   iPSC-CM mathematical model, taking experimental feasibility and throughput into account. To systematically

150   evaluate how different types of data and experimental conditions impact parameter calibration and model

151   predictions of responses to new conditions or drug treatments, we created a simulated *in silico* dataset,

152   generated from a population of Kernik models with random variations in their 16 maximal conductance

153   parameters (Figure 1A, Supplementary Table S2). We simulated AP and CaT generated by these model cells

154   under various conditions (Supplementary Table S3), and then concatenated these data in various

155   combinations based on the "candidate protocols" we wanted to evaluate. The 16 Kernik model conductance

156   parameters were then calibrated, using a genetic algorithm, to best match the steady state AP and CaT traces

157   from each candidate protocol. These fitted parameters were incorporated into the Kernik model, and the newly-

158   calibrated models were evaluated on their ability to predict the original model cell's responses to new

159   conditions (outlined in methods and Figure 1B). Optimizing the experimental protocol using this *in silico* dataset

160   provided 3 major advantages: 1) knowledge of the ground truth parameter values that generated the dataset,

161   so the accuracy of the calibrated parameters can be evaluated, 2) relatively fast and easy simulation of new

162   conditions from the same or additional model cells, in comparison to acquiring new in vitro data and cell lines,

163   and 3) generating corresponding data types through computational methods and data processing, forgoing the

164   need to set up new experiments to collect each data type.
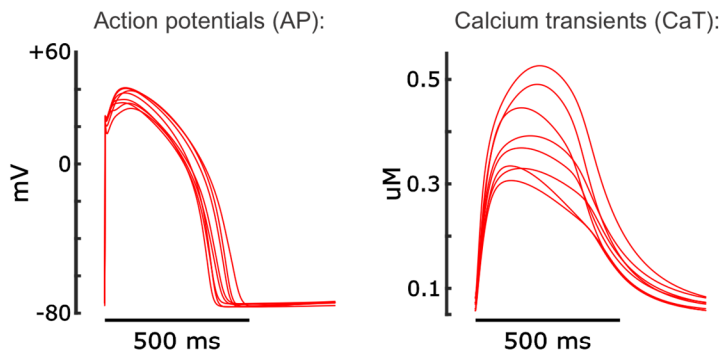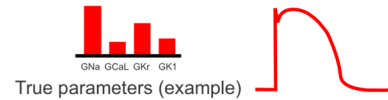
Figure 1: Generation of *in silico* dataset and calibration pipeline optimization. (A) Schematic of the workflow for creating the *in silico* dataset used to optimize the calibration pipeline. (B) Schematic of the genetic algorithm (GA) parameter calibration process, including the true parameters that generated the input data (1), multiple genetic algorithm runs to fit this data (2), and metrics used to evaluate the resulting fitted parameter values (3). The genetic algorithm (GA) creates a population of model cells and simulates the same conditions that generated the input data.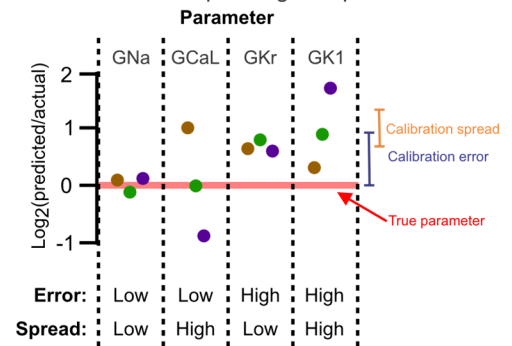 Then, the error between GA-generated traces and input data is calculated to determine how to modify the population, creating a new population. This process is repeated until the population's errors converge (~20 iterations). For parameter evaluation: calibration error = | $\log_2$(fitted parameter value / true parameter value) |; calibration spread = standard deviation of $\log_2$(fitted parameter value / true parameter value) between 10 GA runs.

165

Simultaneously calibrating to AP and CaT data improves model predictions

166

167 First, we examined whether AP or CaT recordings alone provided sufficient information for conductance

168 parameter calibration and model predictions. We used simulated recordings from baseline physiological

169 conditions without pacing stimuli (spontaneous APs), and supplied to a genetic algorithm (GA) either 1) only

170 the AP traces, 2) only the CaT traces, or 3) both (Figure 2A). The GA calibrates parameters by varying them to

9

171   create a population of Kernik model cells, then iteratively selecting and modifying individual models that

172   generated AP and CaT traces that best matched the supplied data (outlined in Figure 1B) [26]. We ran the

173   genetic algorithm 10 times per input dataset, with each GA run starting on a different initial population of

174   models. This allowed us to assess whether each input dataset provided enough information to consistently

175   estimate parameter values, even when the initial search space varied.
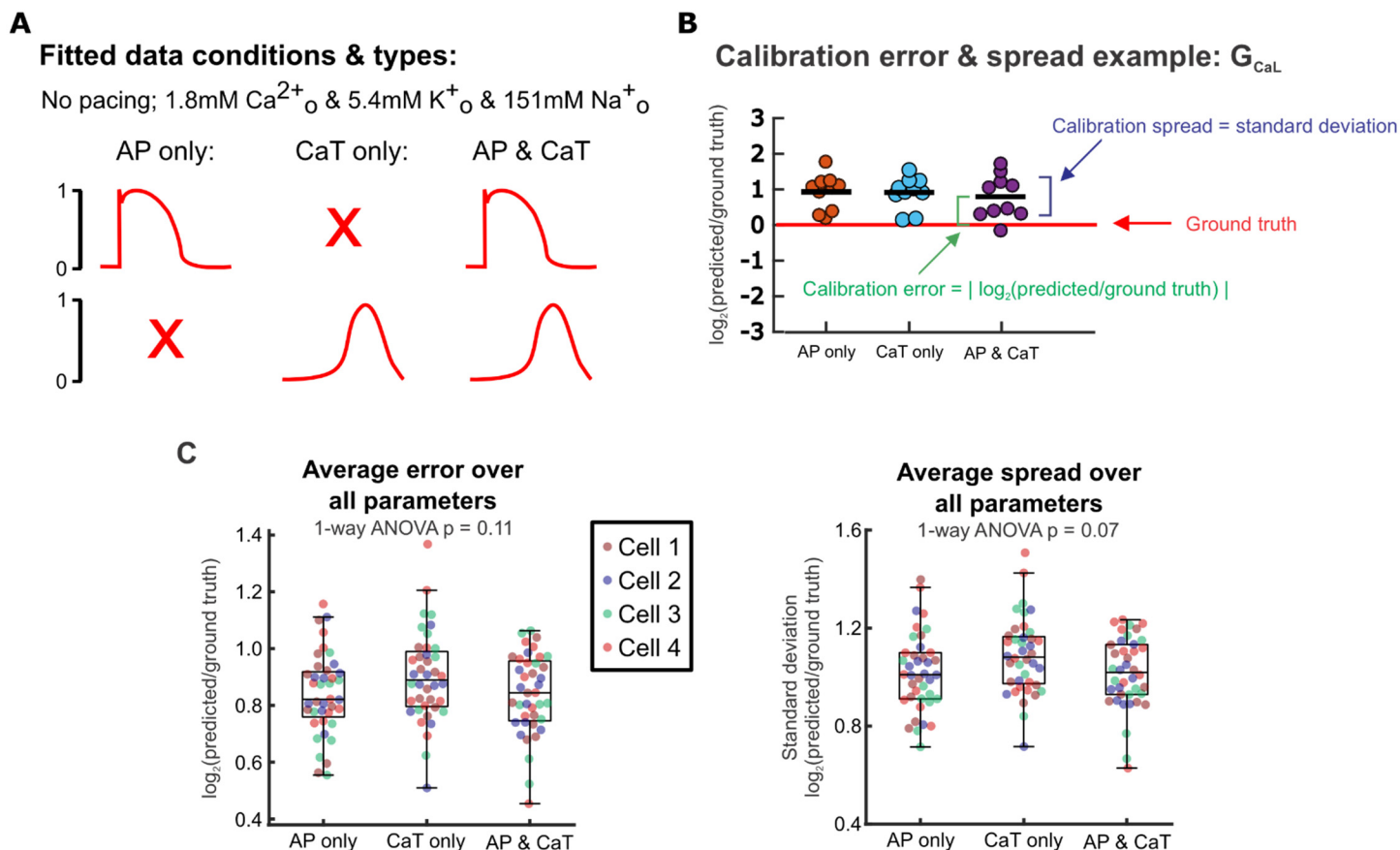

Figure 2: Calibration error and spread remain similar whether only AP, only Ca transient, or both are included during calibration. (A) Schematic of fitted data types. (B) Example of calibrated parameter values from fitting each data type for one parameter (G_{CaL}), log-normalized to the ground truth G_{CaL} value of the fitted model cell. Parameter error and spread calculations are visualized. (C) Parameter errors and spreads calculated by comparing calibrated parameters to the corresponding true parameters of 4 model cells from the *in silico* dataset. Each point represents the average error or spread over all 16 fitted parameters from a single genetic algorithm run for 1 model cell.

177   We evaluated each candidate protocol on parameter calibration accuracy (calibration error) and consistency

178   (calibration spread). Calibration error was represented by the absolute values of calibrated value log-

179   normalized to the corresponding ground truth parameter value, and calibration spread was assessed by

180   calculating the standard deviation (spread) in log-normalized calibrated parameter values between the 10 runs

181   (Figure 2B). After averaging over all 16 fitted parameters, we found minimal differences in calibration error (p =

182   0.11) or spread (p = 0.07) between fitting only voltage, only calcium, or both simultaneously (Figure 2C). From

10

183 these initial tests, therefore, there appears to be little difference between experimental protocols in how well (or

184 poorly) each can identify model parameters.

185 We next assessed the calibrated models from each candidate protocol on how well each predicted model cell

186 responses to 30% block of rapid delayed rectifier current I_{Kr}, as this perturbation is both: 1) independent of the

187 conditions used for model calibration and 2) relevant to cardiac pharmacology [27]. With this evaluation (Figure

188 3A), we found that models fitted to only AP data or only CaT data differed significantly from the ground truth

189 model (Figure 3B, Supplementary Figure S1). When both AP and CaT recordings were used simultaneously

190 during parameter calibration, the resulting calibrated models exhibited substantial improvement in their

191 predictions of 30% I_{Kr} block. Therefore, fitting parameters to both AP and CaT traces simultaneously is

192 required for accurate prediction of results that were not used in the fitting process.
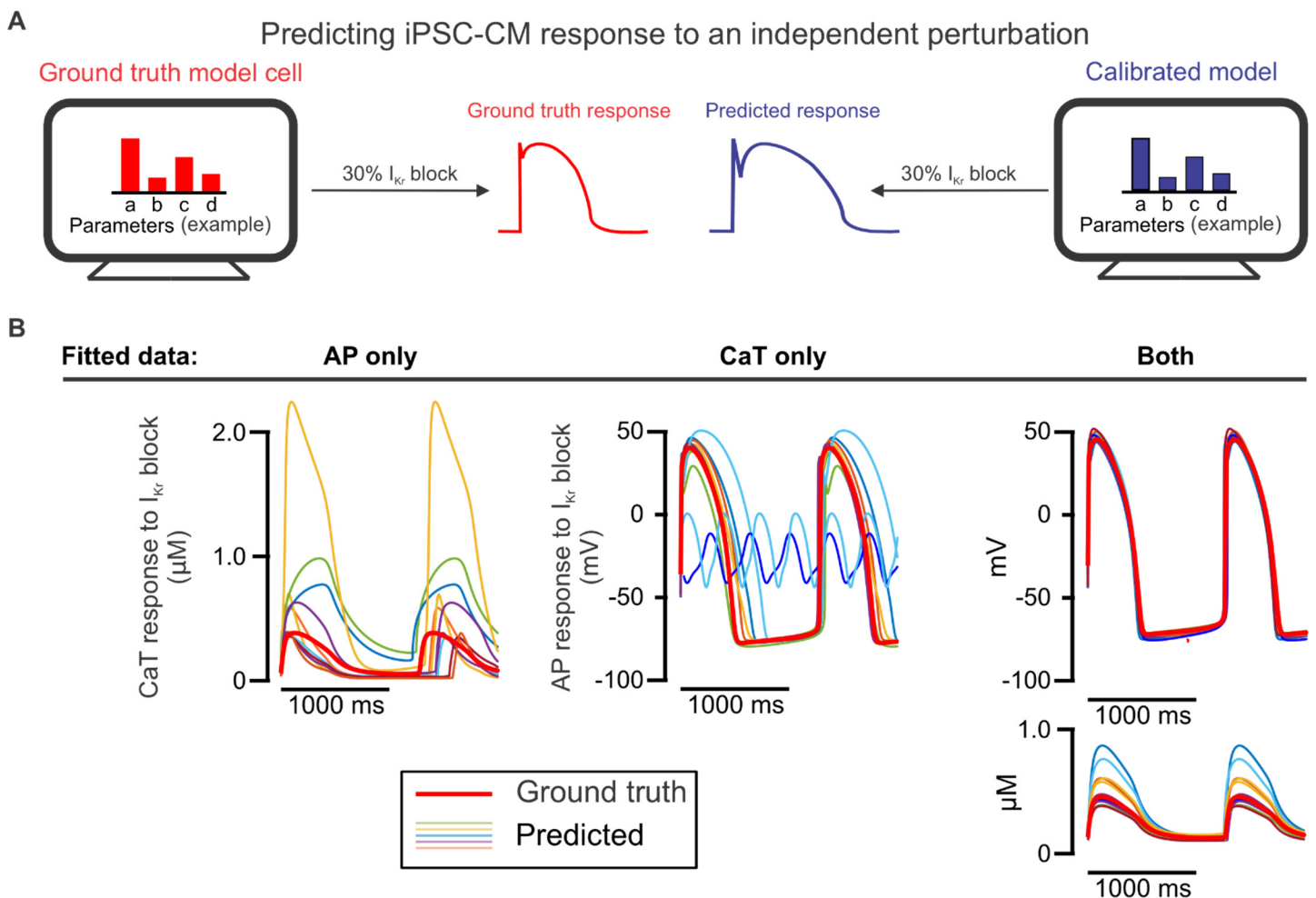
Figure 3: Prediction of iPSC-CM response to an independent perturbation differentiates the models calibrated to AP and CaT simultaneously from those calibrated to single traces. (A) Schematic illustrating the evaluation of calibrated models on their ability to predict an independent response. (B) AP and/or CaT responses to 30% I_{Kr} block predicted by 10 calibrated models for one model cell (thinner traces), compared with the true response of the corresponding model cell (thicker red trace).

193

11

Overall parameter error and spread show minimal change with varied protocol conditions

Next, we explored how varying the number and identity of simulated conditions in the candidate protocols

affected parameter calibration. AP and CaT recordings were simulated under many conditions that could be

produced in an electrophysiology laboratory and constructed candidate protocols from various combinations of

these conditions, which included: 1) varied buffer calcium, from hypo- to normal to hyper-calcemic conditions,

2) spontaneous beating and varied pacing rates from 1-2 Hz, 3) varied levels of L-type calcium channel (I_{CaL})

blockade, and 4) a mixture of these conditions (see Methods for details). We also separated these data into

shorter protocols, to see if the experimental setup could be further simplified (Figure 4A). Unexpectedly, we

found that parameter errors and spread across all 16 maximal conductance parameters did not differ

significantly between the protocols with varied cell culture conditions (Figure 4B, p = 0.814 and p = 0.673,

respectively). Additionally, we observed no significant differences in average calibration errors (p = 0.088) and

spreads (p = 0.137) when varying the number of conditions in the protocol (Figure 4C). Similar findings were

observed when evaluating different combinations of these experimental conditions (Supplementary Figure S2).
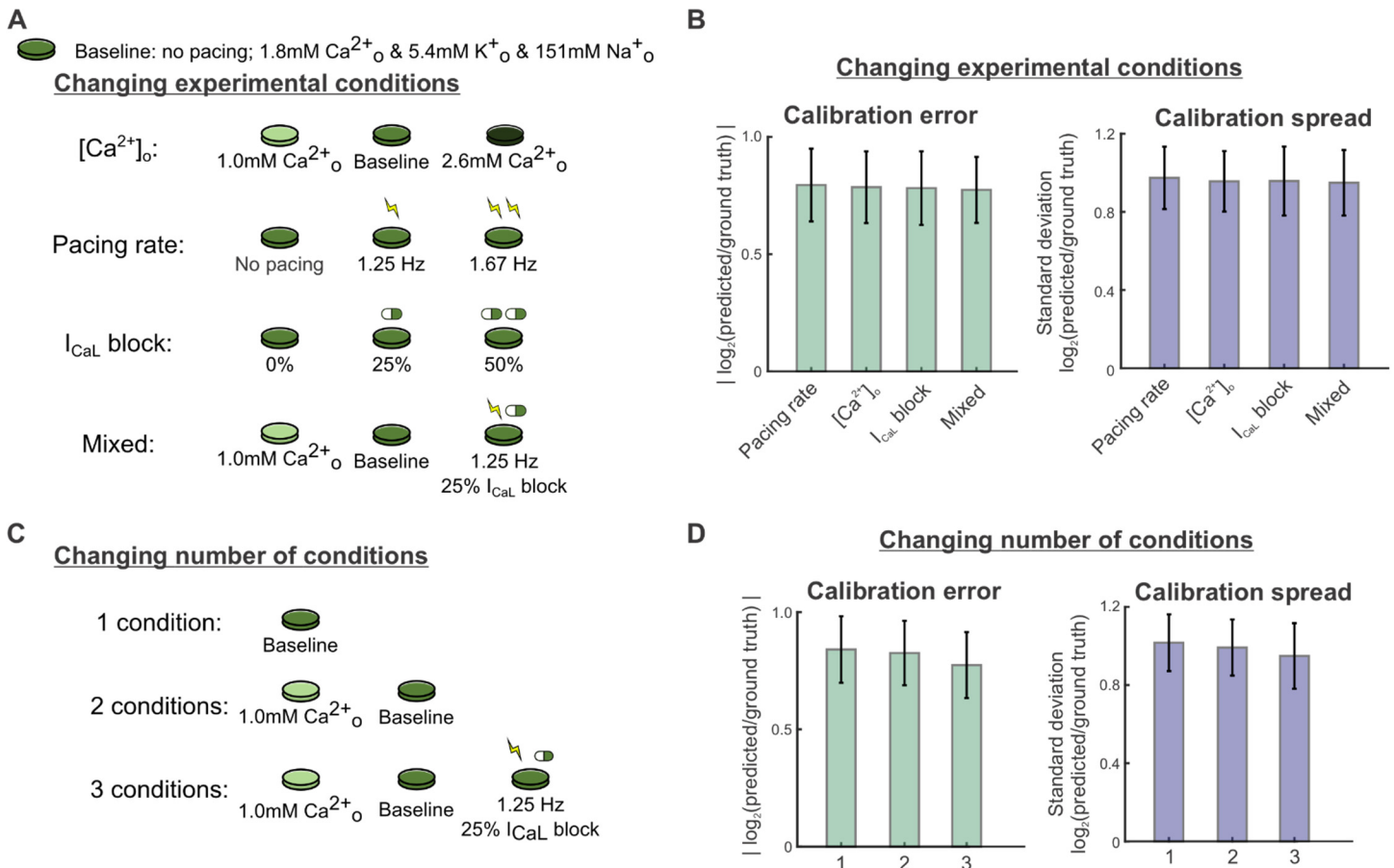
Figure 4: Varying the types and number of experimental conditions has minimal effect on overall calibration error and spread.
(A) Schematic of candidate protocols to generate data for model calibration: varied buffer calcium concentration, varied pacing rates, varied I_{CaL} block levels, and a mixture of the 3. (B) Parameter errors and spreads from calibration runs for 4 Kernik model cells, using calibration data from each protocol in Fig. 4A. Bar plots show the mean calibration errors and spreads over all 16 fitted parameters from 40 calibration runs (10 runs per model cell). Error bars represent standard deviations over these runs. (C) Schematic of candidate protocols to generate data for model calibration: combinations of 1, 2, or 3 parts of the mixed condition protocol. (D) Parameter errors and spreads from calibration runs for 4 Kernik model cells, using calibration data from each protocol in Fig. 4B.

A readily-achievable 3-condition protocol improves predictions of I_{Kr} block response

As with the results shown in Figure 3, we assessed how well calibrated models predicted the response to I_{Kr} block, and we found that accuracy depended strongly on the experimental conditions simulated in each candidate protocol (sample AP traces shown in Figure 5A). Out of the protocols using 3 experimental conditions in Figure 4A, the mixed-conditions protocol generated calibrated models with the most accurate predictions of changes in APs with 30% I_{Kr} block, compared with protocols which varied only the buffer calcium, pacing rates, or I_{CaL} blockade (Figure 5B-C). When evaluating whether a shorter version of this protocol could produce equally predictive models, the full protocol with all 3 conditions outperformed protocols with 1 or 2 of the conditions (Figure 5B-C). These data suggest that an optimal experimental protocol for iPSC-CM model parameter calibration should include voltage and calcium transient fluorescence recordings under at least 3 varieties of cell culture condition changes or perturbations. Of note, this supports our hypothesis that

13

219   data from iPSC-CMs under a variety of conditions provides sufficient parameter identification to generate
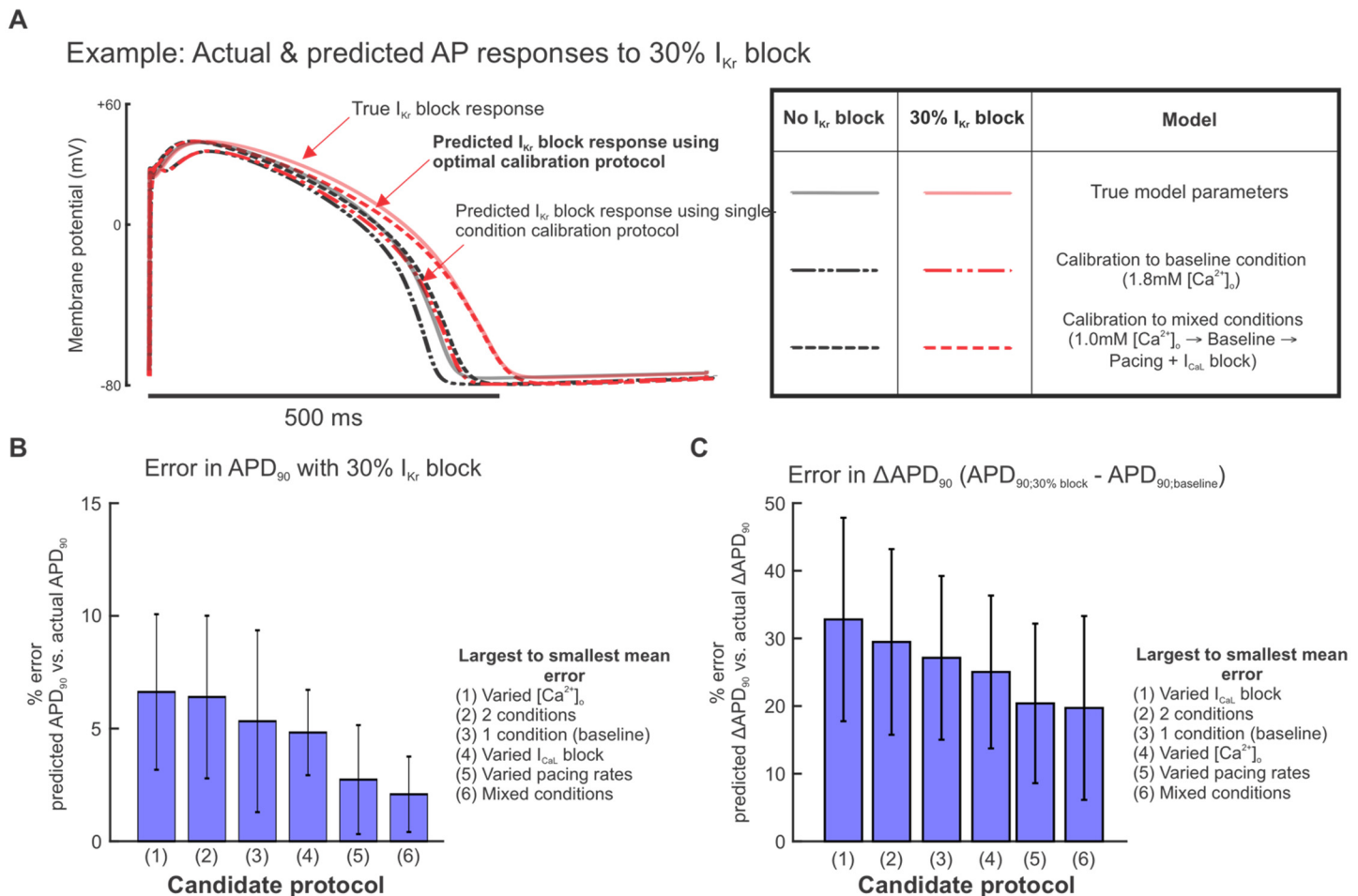
220   predictive models for pharmacological applications.

Figure 5: Calibrating parameters to data from the mixed condition protocol improves model predictions of I_{Kr} block response. (A) Examples of simulated baseline (black graces) and 30% I_{Kr} block (red traces) steady state APs using the ground truth model cell (solid traces) and predicted models (dashed traces) from calibrations to the indicated protocols. (B) Percent error in calibrated model predictions of APD_{90} values at 30% I_{Kr} block. Bars represent means over 10 calibration runs and error bars represent standard deviations. APD_{90} values were normalized to corresponding AP amplitudes before calculating percent error. (C) Percent error in calibrated model predictions of change in APD_{90} change between baseline and 30% I_{Kr} block. APD_{90} values were normalized to corresponding AP amplitudes before calculating percent error.

221

222   **Normalized fluorescence recordings sufficiently inform parameter calibration**

223   Fluorescence recordings generally detect relative changes and do not provide absolute levels of voltage and

224   calcium. Fluorescent dyes can be calibrated [28,29], and patch clamp can detect true transmembrane

225   potentials, but these are more challenging and lower-throughput techniques, compared with straightforward

226   fluorescence recordings. To assess the potential implications for parameter identification, we compared two

227   versions of simulated recordings obtained with our optimized protocol: 1) unscaled (original) *in silico* data,

14

228 representing patch clamp and calibrated calcium measurements, and 2) normalized versions of the same

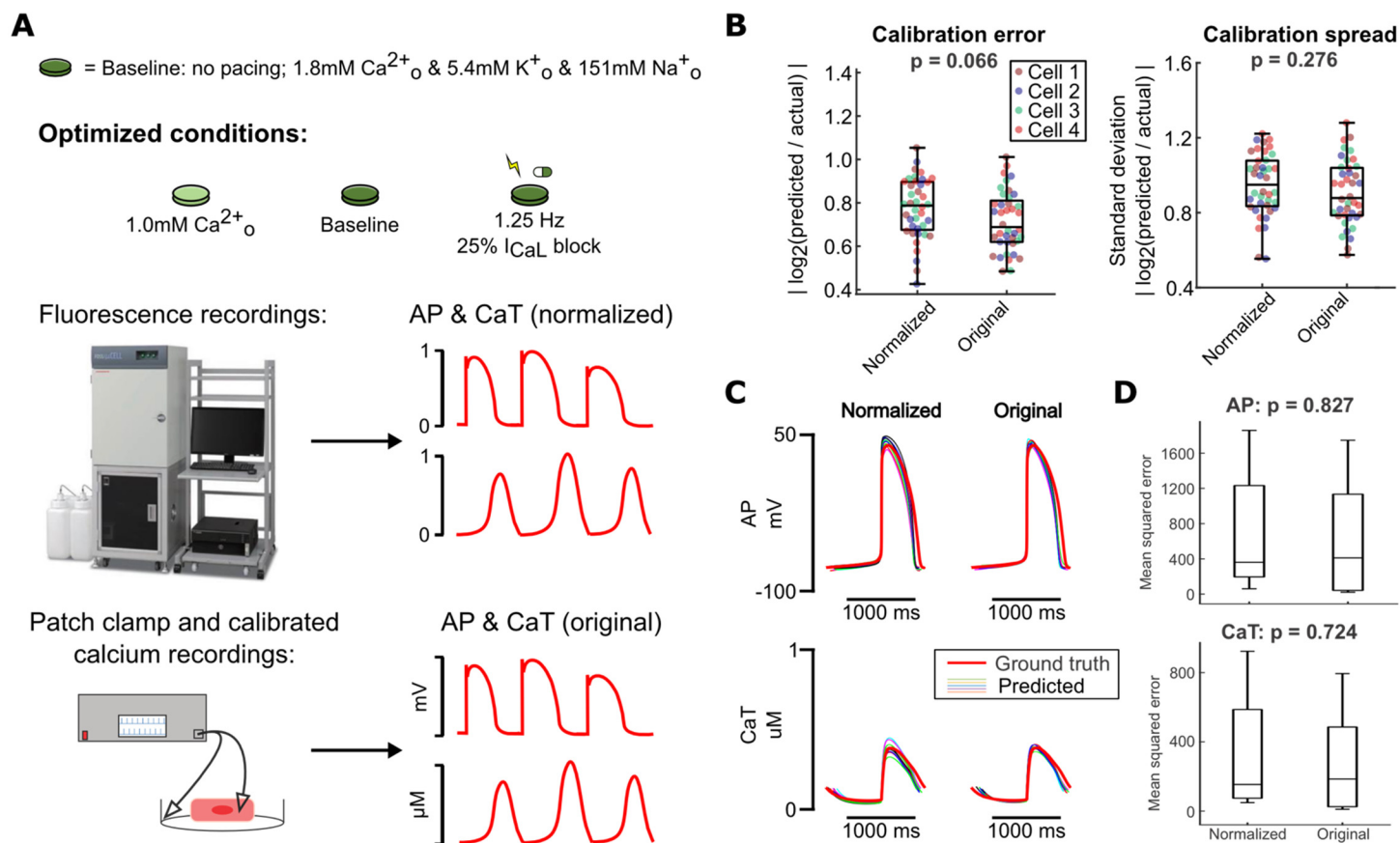229 waveforms, representing simpler fluorescent recordings (Figure 6A).

Figure 6: Normalization of calibration data does not significantly affect model calibration results. (A) Schematic of optimized experimental conditions, normalization of simulated data used to represent fluorescence recordings, and original simulated data used to represent more precise measurement modalities. (B) Parameter errors and spreads from calibration runs on data from 4 Kernik model cells, using either normalized or original data for calibration. Each point represents the average error or spread over all fitted parameters. (C) Predicted AP and CaT responses to 30% I_{Kr} block (thinner traces) from each set of conditions, compared to the true response of the corresponding model cell (thicker red trace). (D) Mean squared errors between data points in the predicted traces (simulated using calibrated models) and the actual model cell's traces, for simulations under 30% I_{Kr} block.

230

231 Parameter calibration accuracy and consistency did not differ significantly when comparing calibrated models

232 from the original data with those from the corresponding normalized data (Figure 6B). Notably, calibrated

233 models from these two data types also performed similarly when evaluating predictions of 30% I_{Kr} block

234 response (Figure 6C). This suggests that fluorescence voltage and calcium recordings from our optimized

235 protocol conditions provide sufficient information to calibrate predictive models.

236 **Calibrated models predict variability in arrhythmia susceptibility *in silico***

237 The primary goal of optimizing a computational pipeline for model calibration is to create cell preparation-

238 specific models that can predict variability in phenotypes, particularly arrhythmia susceptibility, between iPSC-

239 CM lines. To assess the ability of our optimized protocol to predict cell line-specific arrhythmia susceptibility,

15

240   we calculated the lowest level of I_{Kr} block (i.e. highest % I_{Kr}) that induced arrhythmia dynamics

241   (afterdepolarizations, Torsades de Pointes, alternans, beating cessation, or tachycardia) in the same 4 Kernik

242   model cells from our *in silico* dataset. These simulations defined, for each of the 4 model cells, an "I_{Kr} block

243   tolerance threshold" (Figure 7A), which ranged from 37% I_{Kr} block (highest susceptibility) to 62% I_{Kr} block

244   (highest tolerance) (Figure 7C) across the 4 model cells.
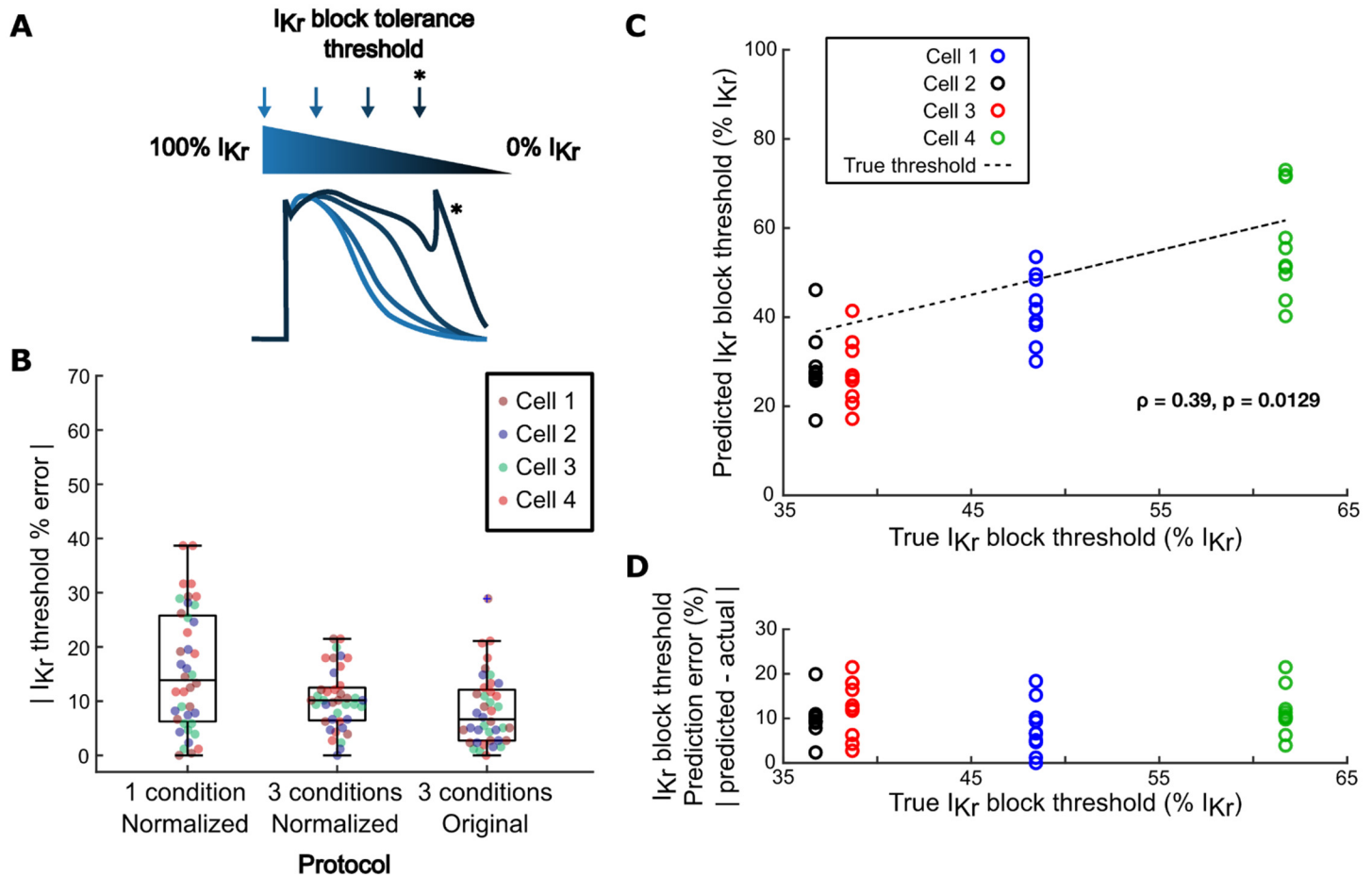
Figure 7: Models generated by the optimized calibration pipeline predict cell-specific arrhythmia susceptibility. (A) Schematic of calculation of I_{Kr} block tolerance threshold. (B) Errors in predictions of I_{Kr} block tolerance threshold, comparing calibrated models from 3 protocols: 1) normalized AP and CaT recordings from a single physiological condition; 2) normalized AP and CaT recordings from the optimized, 3-condition protocol; and 3) non-normalized AP and CaT recordings from the optimized protocol. (C) Correlation between true I_{Kr} block threshold of model cells and their corresponding calibrated models' predicted I_{Kr} block thresholds. (D) Correlation between true I_{Kr} block threshold of model cells and their corresponding calibrated models' I_{Kr} block threshold prediction error.

246   Predicted I_{Kr} block tolerance thresholds were also calculated for the calibrated models generated by our

247   computational pipeline. These predicted thresholds were assessed against the ground truth threshold of the

248   model cell. Calibrated models from our computational pipeline predicted I_{Kr} block thresholds with high accuracy

249   and consistency, with similar error and spread as models calibrated to corresponding non-normalized

250   recordings (Figure 7B). The aggregated calibrated models also predicted relative arrhythmia susceptibility of

16

251 the 4 model cells, as shown by a significant positive correlation between ground truth and predicted I_{Kr} block

252 thresholds in Figure 7C. Additionally, there was no correlation between the model cell's true I_{Kr} block threshold

253 and its associated calibrated models' prediction error, suggesting that the accuracy of these predictions would

254 not be affected by variability in arrhythmia susceptibility between iPSC-CM preparations (Figure 7D).

Optimized model calibration process constrains key ionic parameters

256 Throughout the protocol optimization process, we observed that while calibration error and spread largely

257 remained constant when averaged over all fitted parameters, certain individual parameters consistently

258 showed low calibration spread (e.g. G_{Kr}, G_{NaK}) or high calibration spread (e.g. G_{rel}, G_{CaT}) (Supplementary

259 Figure S3). Thus, we hypothesized that our calibration method only needs to tightly constrain a few key

260 parameters, tolerating inaccuracy or variation in less important parameters while still generating highly

261 predictive calibrated models. To determine whether normalized data from the optimized protocol constrains the

262 parameters that play the largest roles in determining AP and CaT morphology, we analyzed the relationship

263 between parameter calibration accuracy and consistency with the Kernik model's sensitivity to parameter

264 changes. We used multivariable regression to determine how the 16 calibrated model parameters affect

265 relevant phenotypes such as AP duration, CaT amplitude, and I_{Kr} block threshold (Figure 8A) [30]. The

266 resulting model coefficients represent the magnitude and direction of the effect of changes in the

267 corresponding parameter on the modeled phenotype (Figure 8A-C). The most important parameters depended

268 on which model output was considered (Figure 8A-C), but parameters that appeared frequently included rapid

269 delayed rectifier K^+ conductance (G_{Kr}), L-type Ca^{2+} conductance (G_{CaL}), Na^+ conductance (G_{Na}), inward rectifier

270 K^+ conductance (G_{K1}), and Na^+/K^+ pump conductance (G_{NaK}).
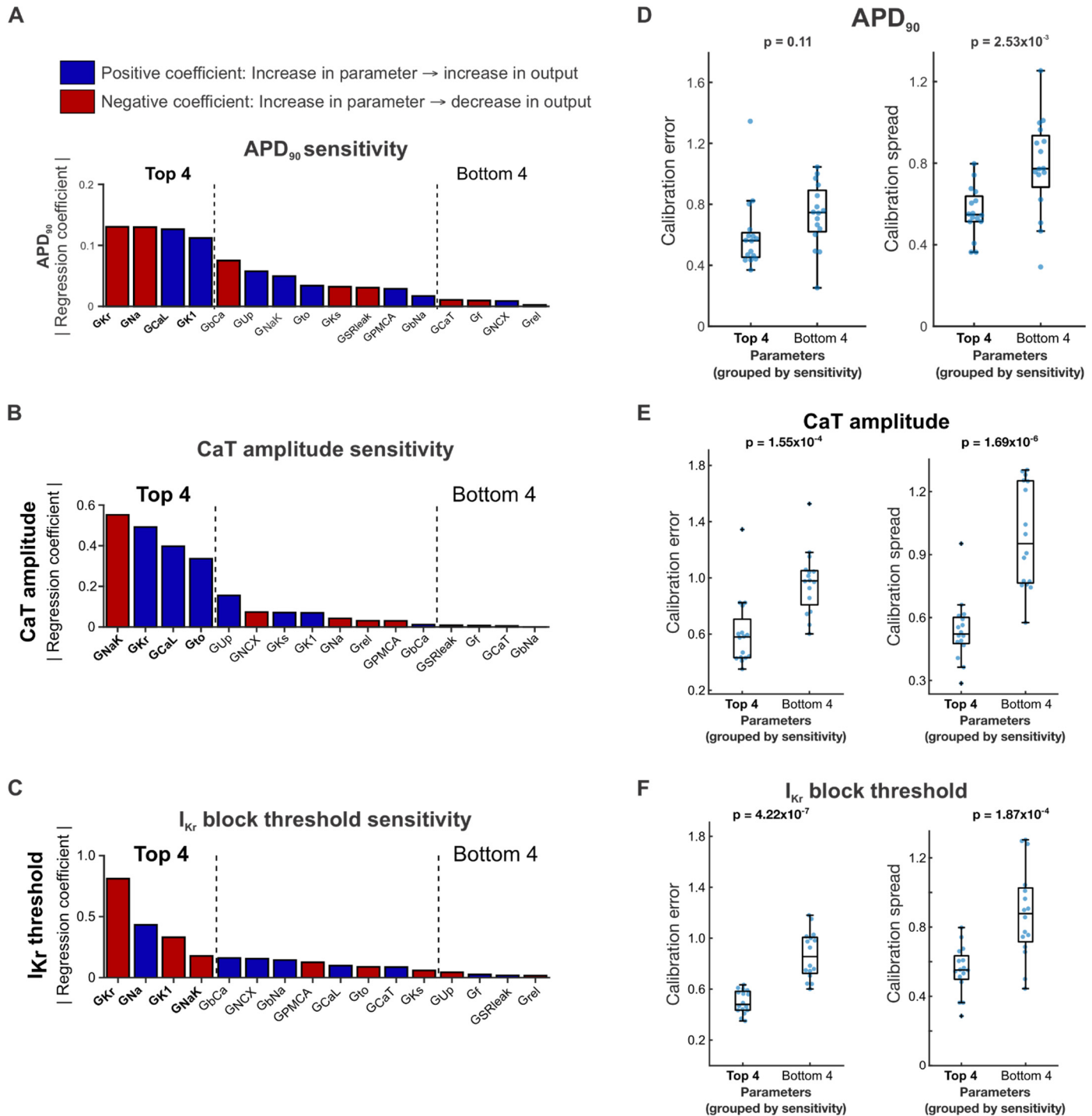
Figure 8: Highly sensitive conductance parameters are well-constrained by the optimized calibration pipeline. (A-C) Regression coefficient magnitudes for each Kernik model maximal conductance parameter's contribution to (A) APD90, (B) CaT amplitude, and (C) I_{Kr} block threshold. Blue bars indicate positive coefficients, and red bars indicate negative coefficients. The top 4 and bottom 4 parameters, ranked by regression coefficient magnitude, are bolded and indicated with black dashed lines. (D-F) Distributions of parameter calibration errors (left) and calibration spread (right) from the optimized calibration pipeline, with parameters grouped into the top 4 and bottom 4 regression coefficient magnitudes for (D) APD90, (E) CaT amplitude, and (F) I_{Kr} block threshold. Each blue dot represents the calibration error or spread value for 1 parameter from calibrations on one model cell (4 parameters per group x 4 model cells = 16 points).

271

272 We then grouped the parameters into the highest and lowest regression coefficient magnitudes for each

273 phenotype, and assessed calibration errors and calibration spreads from the optimized calibration protocol

274 within those groups. The 4 parameters with highest regression coefficient magnitudes for CaT amplitude and

18

275   I_{Kr} block threshold showed significantly lower average calibration error and spread compared with the 4

276   parameters with the lowest regression coefficient magnitudes (Figure 8E-F). Accordingly, the optimized

277   calibration protocol displayed significant improvement over most other candidate protocols in predictions of

278   CaT amplitude and I_{Kr} block threshold. We saw similar results when examining calibration errors and spreads

279   in parameters grouped by APD_{90} sensitivity, though the difference in calibration errors was not statistically

280   significant (Figure 8D). These results suggest that our optimized computational pipeline does constrain the key

281   Kernik model conductance parameters needed to generate predictive models.

282   **Validation of optimized computational pipeline on *in vitro* iPSC-CM recordings**

283   After optimization of our computational pipeline using *in silico* data, where the ground truth model parameter

284   values were known, we assessed whether our pipeline could still generate predictive models using *in vitro*

285   data. We applied the computational pipeline to normalized fluorescence AP and CaT recordings from one

286   iPSC-CM cell line under different combinations of 3 varied conditions: 1) low buffer calcium (1.0 mM) with 1 Hz

287   pacing, 2) physiological buffer calcium (1.8 mM) with 1 Hz pacing, and 3) physiological buffer calcium with 1.25

288   Hz pacing. Figure 9A outlines the data processing and normalization procedures performed on the

289   fluorescence recordings prior to model calibration. Recordings from a separate condition (1.0 mM buffer

290   calcium with 2 Hz pacing) were left out from model calibration, so they could be used to independently

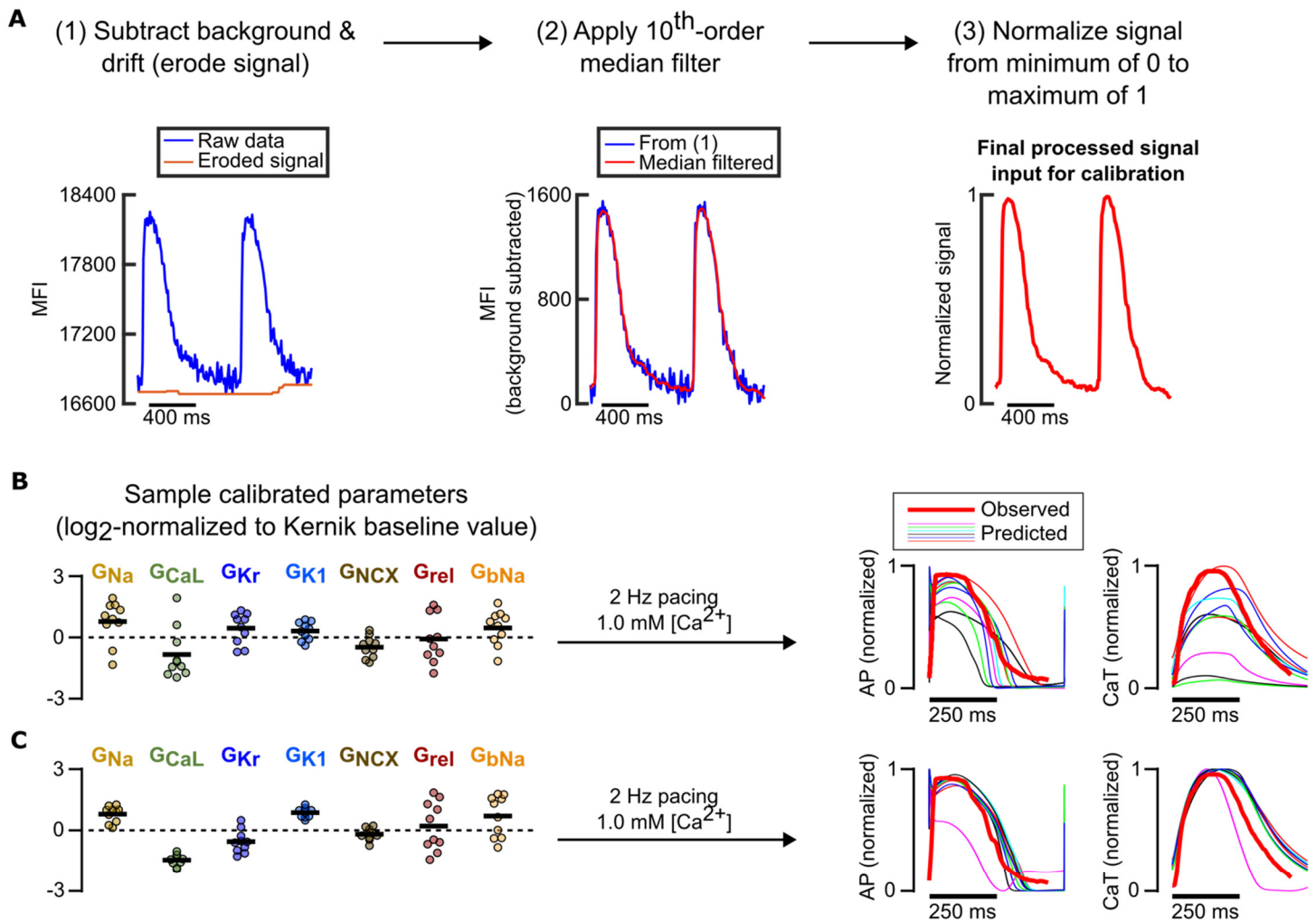291   evaluate predictions generated by the calibrated model.

Figure 9: Preliminary model calibrations to *in vitro* data support findings from *in silico* calibrations. (A) Fluorescence recording processing steps in preparation for model calibration pipeline. (B) Resulting calibrated conductance values (left) normalized to Kernik model baseline values (dashed line at 0) and predicted traces under an independent condition (right) when only data from a single condition (physiological buffer, 1.25 Hz pacing) is used to fit parameters. (C) Resulting calibrated conductance values (left) normalized to Kernik model baseline values (dashed line at 0) and predicted traces under an independent condition (right) when data from varied pacing rates and buffer $[Ca^{2+}]$ are used to fit parameters.

292

293   Calibrating the model conductances using data from only one of these conditions resulted in unconstrained

294   conductance values and highly variable predictions of response to the left-out validation data (Figure 9B).

295   Including data from 2 additional, mixed conditions significantly improved consistency of key conductance

296   parameter calibrations (Figure 9C). When these calibrated parameters were incorporated into the Kernik model

297   and the cell line's response to a new condition was predicted, we found that models calibrated to recordings

298   from 3 conditions substantially outperformed models calibrated to only 1 condition. These results further

299   supported our findings from *in silico* protocol optimization, showing that data from fluorescence voltage and

300   calcium transients under 3 varied conditions can constrain key model parameters and generate predictive, cell

301   preparation-specific models.

DISCUSSION

302

303 While the application of iPSC-derived cardiomyocytes to cardiac disease and pharmacology research has

304 grown dramatically in the past decade, intrinsic and extrinsic variability between cell preparations still hinders

305 reproducibility and clinical translation of studies that use these cells. Generic out-of-box mathematical models

306 of iPSC-CMs do not reflect this variability and potentially generate inaccurate predictions when used to

307 simulate pharmacological ion channel effects or genetic variations [10]. In this study, we aimed to overcome

308 these limitations of the iPSC-CM *in vitro* platform and their mathematical models by creating a computational

309 pipeline which can rapidly identify the cell preparation-specific ionic properties contributing to this phenotypic

310 variability. The parameter calibration algorithm we used, a heuristic genetic algorithm, allows for selection of

311 specific parameters of interest or parameter value limits, and is suitable for parallel computing. To determine

312 the feasibility of this approach, we used a model-generated *in silico* dataset to evaluate candidate protocols

313 containing varied data types and experimental conditions. We found an optimized protocol for fluorescence AP

314 and CaT recordings, consisting of varied buffer calcium concentration, electrical pacing, and I_{CaL} block

315 conditions, which provided enough information to calibrate accurate and predictive cell-specific models, while

316 remaining short in duration and straightforward to acquire. Subsequent model calibrations with an *in vitro*

317 dataset suggested potential flexibility in which specific conditions are selected for the protocol. In our

318 computational pipeline development and subsequent validation, these data were able to inform key ionic

319 contributors, generating calibrated models which accurately and consistently predicted cell-specific responses

320 to I_{Kr} block.

321 **Calibration of models of cardiac electrophysiology**

322 Parameter values in computational models of cardiac electrophysiology are often determined by manual fits to

323 voltage and current recordings, often collected under one or few experimental conditions. This limits the

324 baseline models' ability to represent electrophysiological heterogeneity. Additionally, determination of these

325 baseline parameter values may be affected by selection bias for cells with larger currents, inadequate

326 separation of activation and inactivation kinetics, and inter-laboratory differences in current and voltage clamp

327 protocols [31]. These issues have, in many cases, led researchers to recalibrate the model parameters in

328 attempts to better reflect the behaviors of their specific cardiomyocyte preparations. For example, Potse et al.

21

329   fitted a reaction-diffusion model of ventricular electrical activity to reproduce phenotypes of patients with heart

330   failure or left branch bundle block [32]. Similarly, Lombardo et al. tuned atrial electrophysiology models for

331   patients undergoing ablation therapy [33] whereas Krogh-Madsen et al. used the genetic algorithm to fit a

332   human ventricular cardiac model to clinical QT interval data [34]. In all three cases, these groups found

333   significant discrepancies between the respective initial models and their final, calibrated, fit-for-purpose

334   models. However, to the best of our knowledge, the experimental data used in virtually all previous

335   cardiomyocyte model calibration research come from voltage clamp, patch clamp, or clinical data. Currently,

336   these data are still difficult to obtain from a large group of patients or cell preparations. More recent work has

337   demonstrated the utility of genetic algorithms and the resulting recalibrated models in prediction of arrhythmic

338   behaviors and drug mechanisms, but these also used complex voltage step protocols to calibrate model

339   parameters [35]. These prior results motivated our search for protocols that could calibrate mathematical

340   models using voltage- and calcium-sensitive fluorescent dye measurements, which are considerably easier to

341   acquire than patch-clamp recordings.

342   **Guiding experimental design for optimal parameter calibration**

343   We considered several factors when optimizing the experimental protocol to generate iPSC-CM data for our

344   computational pipeline: 1) the information that the data would provide for parameter calibration, 2) the

345   complexity of the protocol, and 3) the feasibility of the experiment for broad accessibility and high throughput

346   setups. Since the goal of model calibration is usually to improve the accuracy of model parameterizations and

347   predictions, previous work has largely focused on designing experiments to maximize the information content

348   of the resulting data [36–38]. In particular, for cardiac electrophysiology models, model calibration has almost

349   universally been performed on data from complex voltage step protocols, in order to accurately determine

350   individual ion channel conductances and kinetics [10,39,40]. Here, we emphasize that it is also important to

351   identify adaptable protocols that can be widely adopted. Therefore, we opted to focus on using fluorescence

352   recordings to calibrate model parameters, instead of the usual techniques such as patch clamp. To evaluate

353   different protocols, we created an *in silico* dataset for testing various data combinations in their ability to inform

354   parameter calibration. This approach provided 2 major advantages. First, guided by experimental feasibility

355   and relevance, we were able to simulate iPSC-CM electrophysiology under many combinations of conditions

356   without the time and financial costs associated with *in vitro* experiments. Second, we knew the ground truth

22

357 ionic parameter values that produced these AP and CaT traces, so we could precisely assess which simulated

358 conditions informed which parameters. We also ran multiple rounds of genetic algorithms on each tested *in*

359 *silico* protocol, with each round starting from a different initial model population, to assess how consistently

360 each parameter was identified. We used this as a measure of confidence in each parameter estimate.

361 In their analysis on model parameter constraint using regression and Bayesian approaches, Sarkar and Sobie

362 found that, in both cases, parameter constraint improved when values for more than one output feature were

363 provided [41]. Similarly, we found that calibrating model parameters to fluorescence recordings of AP and CaT

364 traces, as opposed to using only one of the two, resulted in better parameter constraint for some (but not all)

365 parameters. Perhaps more importantly, we found that calibrating to both outputs simultaneously resulted in

366 significant improvement of the calibrated models' predictions on a new, independent output. This is consistent

367 with prior results which showed that, when translating drug responses across cell types, using multiple

368 electrophysiological features or observations of iPSC-CMs under multiple conditions improved translations

369 [42–44]. Similarly, our final optimized protocol included a mixture of 3 experimental conditions. Finally, overall

370 parameter calibration accuracy and consistency, as well as independent predictions of I_{Kr} block response, were

371 similar between the models fitted to normalized data (representing fluorescence data) and those fitted to

372 corresponding non-normalized data (representing patch clamp and calibrated Ca^{2+} transient data). Collectively,

373 these findings support our hypothesis that data from fluorescence recordings under multiple conditions, which

374 are more practical compared with microelectrode or patch clamp recordings, can be used to calibrate

375 predictive models. Notably, several parameters such as the background Ca^{2+} and Na^+ conductances, G_{Ks}, and

376 G_{rel} were rarely constrained by any of the datasets we tested. Our subsequent parameter sensitivity analysis

377 showed that model conductances that strongly affect relevant model outputs tend to be well-constrained by our

378 optimized protocol.

379 **Prediction of cell-specific arrhythmia susceptibility**

380 Finally, we demonstrated that our optimized computational pipeline can generate consistent and predictive

381 mathematical models from *in vitro* iPSC-CM data, using fluorescence voltage and calcium recordings under a

382 similar set of experimental conditions. Many therapeutics have the potential to induce patient-specific

383 arrhythmic effects through their intended targets (e.g. quinidine blockade of I_{Na} and I_{Kr}) or unintended effects

23

384 (e.g. antibiotic off-target blockade of K_+ channels) [45,46]. Previous analyses of systems biology models have

385 also argued the importance of a prediction-focused computational modeling approach. In an influential paper,

386 Gutenkunst et al. posited that a model that accurately predicts relevant phenotypes even with some parameter

387 value inaccuracies is more useful than a model with high parameter accuracy and consistency, but inaccurate

388 predictions [47]. This suggests that attempting to determine parameter values directly through precise

389 measurements is an inefficient way of optimizing models. Subsequent studies in both cell signaling and cardiac

390 electrophysiology models have demonstrated success in focusing parameter calibrations on optimizing

391 prediction accuracy in place of specific parameter accuracy [11,48,49]. These analyses demonstrate the

392 importance of calibrating models to not only fit available experimental data, but also generate accurate

393 predictions of responses to novel perturbations.

394 Therefore, while optimizing the computational pipeline, we included a prediction metric in addition to parameter

395 value accuracy and consistency. We created a quantifiable, pharmacologically-relevant measure of cell-

396 specific arrhythmia susceptibility by finding the lowest level of I_{Kr} block that induced arrhythmic dynamics in

397 each Kernik model (*in silico*) or iPSC-CM preparation (*in vitro*), which we termed the "I_{Kr} block tolerance

398 threshold". Calibrated models from our optimized computational pipeline were able to predict this threshold

399 consistently and accurately, with similar error as those from calibrating to the original, non-normalized data.

400 The models calibrated to normalized data were also able to correctly rank the I_{Kr} block arrhythmia

401 susceptibilities of the fitted Kernik model cells, suggesting that the models generated by this pipeline contain

402 enough information to predict cell-specific arrhythmia susceptibilities, despite errors and non-constraint of

403 several smaller conductance parameters.

Limitations and potential directions

405 The model calibration process developed and optimized in this study can be applied broadly to research that

406 investigates the ionic mechanisms behind iPSC-CM phenotype variability or predicts differential effects of

407 therapeutics on various iPSC-CM cell lines and preparations. However, phenotypic variability also exists within

408 iPSC-CMs from the same preparation. While it is possible to use fluorescent dyes to record electrophysiology

409 of individual cells, we currently focused our efforts on calibrating models to represent multicellular preparations.

24

410 Future work could include adapting this computational pipeline to calibrate models representing single

411 cardiomyocytes within an iPSC-CM preparation.

412 Several conductance parameters fitted in our current pipeline did not contribute significantly to

413 electrophysiological phenotype and responses (e.g. G_f, G_{SRleak}, and G_{rel}), according to our parameter sensitivity

414 analyses. Many of these same parameters were also less accurate and less constrained by our computational

415 pipeline. While we showed that the resulting calibrated models could accurately predict several major

416 electrophysiology phenotypes and channel block responses, we do not know whether these models could still

417 predict responses that are strongly affected by one or more of the unconstrained parameters. Calibrated

418 models generated by our computational pipeline should be evaluated on their ability to predict cell-specific

419 susceptibility to other pro- or anti-arrhythmia triggers of interest, such as I_{CaL} or buffer $[K^+]$ changes. If

420 improving parameter calibration accuracy and constraint of particular ionic current(s) is found to be necessary

421 for model predictive power, one option would be to replace the conductances with lowest parameter sensitivity

422 regression coefficient magnitudes with representative kinetic parameters, such as time constants or activation

423 gates. If these kinetic parameters are found to impact electrophysiology in a manner that is detectable by the

424 genetic algorithm, their calibrations will likely be more accurate and constrained, generating more precise cell

425 preparation-specific iPSC-CM models.

426 **Conclusions**

427 The optimized model calibration computational pipeline we developed in this study can be applied to ongoing

428 pharmacological and disease studies to understand cell response variability in iPSC-CMs and advance

429 precision medicine. Our pipeline simultaneously fits multiple model parameters to fluorescence voltage and

430 calcium recordings, which are quicker and simpler to acquire than the patch clamp or other more involved

431 electrophysiological techniques used in prior model calibration work. The ability to use fluorescence recordings

432 increases this pipeline's accessibility and throughput compared to prior methods. This unique characteristic

433 makes our computational pipeline suitable for rapid generation of cell-specific models for therapeutic, disease,

434 or population studies. Comparing cell-specific model parameters between iPSC-CM cell lines or to a

435 benchmark, such as an adult cardiac model, would reveal ionic mechanisms behind this variability in iPSC-CM

436 maturation and phenotypes. In addition, the personalized models created by this computational pipeline can

25

437   simulate patient-specific drug and perturbation responses to quickly predict therapeutic efficacy or drug

438   cardiotoxicity. In future studies, these calibrated iPSC-CM models can inform translation of ionic properties and

439   physiological responses into adult cardiac models, which could, in turn, generate even more accurate,

440   clinically-relevant cardiac electrophysiology phenotype and drug response predictions.

METHODS

Simulations of iPSC-CM electrophysiology

In silico simulations of iPSC-CM electrophysiology (e.g. membrane potential, calcium transients, changes in maximal conductances and ionic currents) were carried out in MATLAB R2020b by solving the ordinary differential equations defined in the Kernik et al. (2019) mathematical model of human iPSC-CMs [9], using the initial conditions listed in Supplementary Table S1. In cases where a protocol included cardiomyocyte pacing, electrical stimuli of 60 pA/pF were simulated for a duration of 1 ms at the specified intervals. All simulations were run for 5 minutes, which was sufficient to achieve a steady state using the baseline model and physiological, unperturbed conditions (Supplementary Table S3, protocol #19). The voltage and intracellular calcium concentration from the final 5 seconds of each simulation were stored and included in the *in silico* dataset.

In silico dataset for optimization of iPSC-CM experimental protocol

To simulate a heterogeneous set of iPSC-CM cell lines, a "population" of Kernik model cells was created by drawing multiplier factors for each maximal conductance parameter from a log-normal distribution with mean multiplier = 1, spread = 0.2. This population was then simulated under physiological, unperturbed conditions (Supplementary Table S3, protocol 19), and filtered for cells which showed a spontaneous beating frequency between 0.3 Hz and 1.0 Hz, nearly matching the automaticity rate range for human iPSC-CMs reported in [50]. Out of the remaining model cells, 4 were randomly selected for simulation under the 19 different conditions, to generate the final *in silico* dataset. The Kernik model's baseline conductance parameter values and the scaled conductances for these 4 model cells are listed in Supplementary Table S2. A list of the various conditions these 4 cells were simulated under can be found in Supplementary Table S3. All simulations were run for a 5-minute time span (steady state under physiological buffer conditions, without pacing), and membrane potential and intracellular calcium recordings from the final 5 seconds of these simulations were extracted and stored for the *in silico* dataset. The built-in *interp1* function in MATLAB was used to interpolate these data in equal time steps (0.1 ms). To mimic processed data from fluorescence recordings, we also created "normalized" versions of each dataset by scaling the data from a minimum of 0 to a maximum of 1. This dataset allowed for

467 comparison of conductance parameter estimates produced during model calibration against known ground

468 truth conductance values.

Parameter calibration using the genetic algorithm

470 The data used for calibrating model parameters included the steady state AP and CaT waves from the

471 previously-generated *in silico* dataset. Individual simulation runs are either included or excluded from the fitting

472 procedure to compare different experimental "candidate protocols". Rapid delayed rectifier potassium current

473 (I_{Kr}) block conditions were left out from protocol optimization to use for conductance estimate validation. If the

474 candidate protocol consists of more than 1 condition, the final values of membrane potential, intracellular

475 calcium concentration, and other steady state parameters are used as the starting values for the subsequent

476 protocol condition. To determine the optimal protocol for accurate and consistent parameter identification,

477 Kernik model maximal conductance parameters were fitted to *in silico* from each candidate protocol simulated

478 for 4 of the dataset's model cells, using the genetic algorithm (GA) [10,12]. Briefly, the GA creates a new

479 population of Kernik model cells, each randomly assigned a set of conductance parameter scale factors, and

480 simulates the candidate protocol for each of these model cells. Then, the mean squared error between

481 corresponding data points in the GA-generated trace and the trace from the *in silico* dataset is calculated. The

482 model cells with the lowest errors are retained, while higher-scoring cells have their parameter values altered

483 in the next algorithm iteration. Details about specific GA settings, such as population size and parameter

484 retention/alteration criteria, can be found in Supplementary Table S4. This process repeats for 20 iterations,

485 where each new population has a lower average error than the previous. The parameters of the model cell with

486 the lowest error from the final population are selected as the final calibrated parameter values from that run.

487 Parameter calibrations are conducted 10 times per candidate protocol per model cell, with each of the 10 GA

488 runs starting with a different set of initial model populations. The 10 sets of conductance estimates from each

489 GA run are evaluated on 1) accuracy to the ground truth parameter values of the model cells and 2) ability to

490 predict the model cell's response to a perturbation that was not seen during parameter calibration, such as I_{Kr}

491 block.

***In vitro* iPSC-CM tissue culture and optical recordings**

493 Human induced pluripotent stem cells (iPSCs) derived from a single cell line were differentiated into

28

494 cardiomyocytes (iPSC-CMs) by modulating canonical Wnt signaling [51]. The cardiomyocytes were enriched,

495 then combined with cardiac fibroblasts in a ratio of 90% iPSC-CMs to 10% fibroblasts within a collagen-fibrin

496 hydrogel solution (InvivoSciences, Inc., Madison, WI, USA). The engineered heart tissues (EHTs) thus formed

497 were maintained in a serum-free cardiac maintenance medium, supplemented with penicillin and streptomycin

498 (Thermo Fisher Scientific, Waltham, MA, USA), within 96-well micro culture plates (MC-96, InvivoSciences).

499 EHT maintenance was carried out as previously described in relevant literature [52]. Following a five-day

500 remodeling phase, the EHTs underwent further maturation with biphasic constant current electrical stimulations

501 at a frequency of 1Hz for 8 days.

502 For optical voltage and calcium transient recordings, the EHTs were loaded with Fluovolt (at a dilution of 1:500,

503 Thermo Fisher Scientific), or Cal-520 AM (also at 1:500, AAT Bioquest), along with PowerLoad (Thermo Fisher

504 Scientific), by incubating them for one hour in Tyrode's solution. This solution was prepared with either 1.0 mM

505 or 1.8 mM [Ca^{2+}]. Following the removal of the dyes, the solution was pH adjusted to 7.4 and warmed, and

506 Tyrode's solution with the corresponding calcium concentration was reintroduced to aid in recovery from dye

507 loading stress over a 30-minute period. The EHTs were then paced at frequencies of 1.0 Hz, 1.25 Hz, or 2.0

508 Hz for five minutes. The steady-state membrane potential and intracellular calcium transients during this period

509 were recorded using a high-throughput fluorescence plate imager, FDSS/µCell (Hamamatsu Photonics K.K.,

510 Japan), utilizing 470nm excitation and 540nm emission at a rate of 125 data points per second. The collected

511 data were analyzed with the iVSurfer™ software (InvivoSciences), specifically designed for high-throughput

512 waveform data analysis.

513 **Processing of *in vitro* iPSC-CM recordings for the computational pipeline**

514 Fluorescence voltage and calcium recordings were processed in MATLAB with baseline drift subtraction

515 (imerode function), median filtering to remove noise (medfilt1 function), and the same normalization steps as

516 the pseudo-data. Kernik model maximal conductance parameters were fitted to these data using the same

517 workflow as prior fittings to pseudo-data, with the 1.0mM buffer [Ca^{2+}], 2.0Hz pacing data left out for validation.

REFERENCES

1. Karakikes I, Ameen M, Termglinchan V, Wu JC. Human Induced Pluripotent Stem Cell-Derived Cardiomyocytes: Insights into Molecular, Cellular, and Functional Phenotypes. Circ Res. 2015;117: 80–88. doi:10.1161/CIRCRESAHA.117.305365

2. Huang C-Y, Liu C-L, Ting C-Y, Chiu Y-T, Cheng Y-C, Nicholson MW, et al. Human iPSC banking: barriers and opportunities. J Biomed Sci. 2019;26: 87. doi:10.1186/s12929-019-0578-x

3. Hnatiuk AP, Briganti F, Staudt DW, Mercola M. Human iPSC modeling of heart disease for drug development. Cell Chem Biol. 2021;28: 271–282. doi:10.1016/j.chembiol.2021.02.016

4. Yang J, Argenziano MA, Burgos Angulo M, Bertalovitz A, Beidokhti MN, McDonald TV. Phenotypic Variability in iPSC-Induced Cardiomyocytes and Cardiac Fibroblasts Carrying Diverse LMNA Mutations. Front Physiol. 2021;12: 778982. doi:10.3389/fphys.2021.778982

5. Nakagawa M, Ooie T, Ou B, Ichinose M, Takahashi N, Hara M, et al. Gender differences in autonomic modulation of ventricular repolarization in humans. J Cardiovasc Electrophysiol. 2005;16: 278–284. doi:10.1046/j.1540-8167.2005.40455.x

6. Paci M, Hyttinen J, Aalto-Setälä K, Severi S. Computational models of ventricular- and atrial-like human induced pluripotent stem cell derived cardiomyocytes. Ann Biomed Eng. 2013;41: 2334–2348. doi:10.1007/s10439-013-0833-3

7. Koivumäki JT, Naumenko N, Tuomainen T, Takalo J, Oksanen M, Puttonen KA, et al. Structural Immaturity of Human iPSC-Derived Cardiomyocytes: In Silico Investigation of Effects on Function and Disease Modeling. Front Physiol. 2018;9: 80. doi:10.3389/fphys.2018.00080

8. Paci M, Pölönen R-P, Cori D, Penttinen K, Aalto-Setälä K, Severi S, et al. Automatic Optimization of an in Silico Model of Human iPSC Derived Cardiomyocytes Recapitulating Calcium Handling Abnormalities. Front Physiol. 2018;9: 709. doi:10.3389/fphys.2018.00709

9. Kernik DC, Morotti S, Wu H, Garg P, Duff HJ, Kurokawa J, et al. A computational model of induced pluripotent stem-cell derived cardiomyocytes incorporating experimental variability from multiple data sources. J Physiol. 2019;597: 4533–4564. doi:10.1113/JP277724

10. Groenendaal W, Ortega FA, Kherlopian AR, Zygmunt AC, Krogh-Madsen T, Christini DJ. Cell-Specific Cardiac Electrophysiology Models. PLoS Comput Biol. 2015;11: e1004242. doi:10.1371/journal.pcbi.1004242

11. Dokos S, Lovell NH. Parameter estimation in cardiac ionic models. Prog Biophys Mol Biol. 2004;85: 407–431. doi:10.1016/j.pbiomolbio.2004.02.002

12. Syed Z, Vigmond E, Nattel S, Leon LJ. Atrial cell action potential parameter fitting using genetic algorithms. Med Biol Eng Comput. 2005;43: 561–571. doi:10.1007/BF02351029

13. Devenyi RA, Ortega FA, Groenendaal W, Krogh-Madsen T, Christini DJ, Sobie EA. Differential roles of two delayed rectifier potassium currents in regulation of ventricular action potential duration and arrhythmia susceptibility. J Physiol. 2017;595: 2301–2317. doi:10.1113/JP273191

14. Akwaboah AD, Tsevi B, Yamlome P, Treat JA, Brucal-Hallare M, Cordeiro JM, et al. An in silico hiPSC-Derived Cardiomyocyte Model Built With Genetic Algorithm. Front Physiol. 2021;12: 675867. doi:10.3389/fphys.2021.675867

15. Beattie KA, Hill AP, Bardenet R, Cui Y, Vandenberg JI, Gavaghan DJ, et al. Sinusoidal voltage protocols for rapid characterisation of ion channel kinetics. J Physiol. 2018;596: 1813–1828. doi:10.1113/JP275733

16. Ahmed RE, Anzai T, Chanthra N, Uosaki H. A Brief Review of Current Maturation Methods for Human Induced Pluripotent Stem Cells-Derived Cardiomyocytes. Front Cell Dev Biol. 2020;8. Available: https://www.frontiersin.org/article/10.3389/fcell.2020.00178

17. Karbassi E, Fenix A, Marchiano S, Muraoka N, Nakamura K, Yang X, et al. Cardiomyocyte maturation: advances in knowledge and implications for regenerative medicine. Nat Rev Cardiol. 2020;17: 341–359. doi:10.1038/s41569-019-0331-x

18. James EC, Tomaskovic-Crook E, Crook JM. Bioengineering Clinically Relevant Cardiomyocytes and Cardiac Tissues from Pluripotent Stem Cells. Int J Mol Sci. 2021;22: 3005. doi:10.3390/ijms22063005

19. Guo Y, Pu W. Cardiomyocyte Maturation: New Phase in Development. Circ Res. 2020;126: 1086–1106. doi:10.1161/CIRCRESAHA.119.315862

20. Mannhardt I, Saleem U, Mosqueira D, Loos MF, Ulmer BM, Lemoine MD, et al. Comparison of 10 Control hPSC Lines for Drug Screening in an Engineered Heart Tissue Format. Stem Cell Rep. 2020;15: 983–998. doi:10.1016/j.stemcr.2020.09.002

21. Lauschke K, Volpini L, Liu Y, Vinggaard AM, Hall VJ. A Comparative Assessment of Marker Expression Between Cardiomyocyte Differentiation of Human Induced Pluripotent Stem Cells and the Developing Pig Heart. Stem Cells Dev. 2021;30: 374–385. doi:10.1089/scd.2020.0184

22. Yang X, Pabon L, Murry CE. Engineering Adolescence: Maturation of Human Pluripotent Stem Cell-derived Cardiomyocytes. Circ Res. 2014;114: 511–523. doi:10.1161/CIRCRESAHA.114.300558

23. Yoshida Y, Yamanaka S. Induced Pluripotent Stem Cells 10 Years Later. Circ Res. 2017;120: 1958–1968. doi:10.1161/CIRCRESAHA.117.311080

24. Kannan S, Farid M, Lin BL, Miyamoto M, Kwon C. Transcriptomic entropy benchmarks stem cell-derived cardiomyocyte maturation against endogenous tissue at single cell level. PLoS Comput Biol. 2021;17: e1009305. doi:10.1371/journal.pcbi.1009305

25. Grancharova T, Gerbin KA, Rosenberg AB, Roco CM, Arakaki JE, DeLizo CM, et al. A comprehensive analysis of gene expression changes in a high replicate and open-source dataset of differentiating hiPSC-derived cardiomyocytes. Sci Rep. 2021;11: 15845. doi:10.1038/s41598-021-94732-1

26. Wang F-S, Chen L-H. Heuristic Optimization. In: Dubitzky W, Wolkenhauer O, Cho K-H, Yokota H, editors. Encyclopedia of Systems Biology. New York, NY: Springer; 2013. pp. 885–885. doi:10.1007/978-1-4419-9863-7_411

27. Carusi A, Burrage K, Rodríguez B. Bridging experiments, models and simulations: an integrative approach to validation in computational cardiac electrophysiology. Am J Physiol-Heart Circ Physiol. 2012;303: H144–H155. doi:10.1152/ajpheart.01151.2011

28. Grynkiewicz G, Poenie M, Tsien RY. A new generation of Ca2+ indicators with greatly improved fluorescence properties. J Biol Chem. 1985;260: 3440–3450. doi:10.1016/S0021-9258(19)83641-4

29. Bräuner T, Hülser DF, Strasser RJ. Comparative measurements of membrane potentials with microelectrodes and voltage-sensitive dyes. Biochim Biophys Acta BBA - Biomembr. 1984;771: 208–216. doi:10.1016/0005-2736(84)90535-2

30. Sobie EA. Parameter Sensitivity Analysis in Electrophysiological Models Using Multivariable Regression. Biophys J. 2009;96: 1264–1274. doi:10.1016/j.bpj.2008.10.056

31. Krogh-Madsen T, Sobie EA, Christini DJ. Improving cardiomyocyte model fidelity and utility via dynamic electrophysiology protocols and optimization algorithms. J Physiol. 2016;594: 2525–2536. doi:10.1113/JP270618

32. Potse M, Krause D, Kroon W, Murzilli R, Muzzarelli S, Regoli F, et al. Patient-specific modelling of cardiac electrophysiology in heart-failure patients. Europace. 2014;16: iv56–iv61. doi:10.1093/europace/euu257

33. Lombardo DM, Fenton FH, Narayan SM, Rappel W-J. Comparison of Detailed and Simplified Models of Human Atrial Myocytes to Recapitulate Patient Specific Properties. PLOS Comput Biol. 2016;12: e1005060. doi:10.1371/journal.pcbi.1005060

34. Krogh-Madsen T, Jacobson AF, Ortega FA, Christini DJ. Global Optimization of Ventricular Myocyte Model to Multi-Variable Objective Improves Predictions of Drug-Induced Torsades de Pointes. Front Physiol. 2017;8. Available: https://www.frontiersin.org/articles/10.3389/fphys.2017.01059

35. Clark AP, Wei S, Kalola D, Krogh-Madsen T, Christini DJ. An in silico–in vitro pipeline for drug cardiotoxicity screening identifies ionic pro-arrhythmia mechanisms. Br J Pharmacol. 2022;179: 4829–4843. doi:10.1111/bph.15915

36. Liepe J, Filippi S, Komorowski M, Stumpf MPH. Maximizing the Information Content of Experiments in Systems Biology. PLOS Comput Biol. 2013;9: e1002888. doi:10.1371/journal.pcbi.1002888

37. Chaloner K, Verdinelli I. Bayesian Experimental Design: A Review. Stat Sci. 1995;10: 273–304. doi:10.1214/ss/1177009939

38. Ryan EG, Drovandi CC, McGree JM, Pettitt AN. A Review of Modern Computational Algorithms for Bayesian Optimal Design. Int Stat Rev. 2016;84: 128–154. doi:10.1111/insr.12107

39. Whittaker DG, Clerx M, Lei CL, Christini DJ, Mirams GR. Calibration of ionic and cellular cardiac electrophysiology models. Wiley Interdiscip Rev Syst Biol Med. 2020;12: e1482. doi:10.1002/wsbm.1482

40. Lei CL, Clerx M, Beattie KA, Melgari D, Hancox JC, Gavaghan DJ, et al. Rapid Characterization of hERG Channel Kinetics II: Temperature Dependence. Biophys J. 2019;117: 2455–2470. doi:10.1016/j.bpj.2019.07.030

41. Sarkar AX, Sobie EA. Regression Analysis for Constraining Free Parameters in Electrophysiological Models of Cardiac Cells. PLOS Comput Biol. 2010;6: e1000914. doi:10.1371/journal.pcbi.1000914

42. Gong JQX, Sobie EA. Population-based mechanistic modeling allows for quantitative predictions of drug responses across cell types. Npj Syst Biol Appl. 2018;4: 1–11. doi:10.1038/s41540-018-0047-2

43. Tveito A, Jæger KH, Huebsch N, Charrez B, Edwards AG, Wall S, et al. Inversion and computational maturation of drug response using human stem cell derived cardiomyocytes in microphysiological systems. Sci Rep. 2018;8: 17626. doi:10.1038/s41598-018-35858-7

44. Morotti S, Liu C, Hegyi B, Ni H, Fogli Iseppe A, Wang L, et al. Quantitative cross-species translators of cardiac myocyte electrophysiology: Model training, experimental validation, and applications. Sci Adv. 2021;7: eabg0927. doi:10.1126/sciadv.abg0927

45. Kannankeril PJ, Roden DM, Norris KJ, Whalen SP, George AL, Murray KT. Genetic susceptibility to acquired long QT syndrome: Pharmacologic challenge in first-degree relatives. Heart Rhythm. 2005;2: 134–140. doi:10.1016/j.hrthm.2004.10.039

46. Zequn Z, Yujia W, Dingding Q, Jiangfang L. Off-label use of chloroquine, hydroxychloroquine, azithromycin and lopinavir/ritonavir in COVID-19 risks prolonging the QT interval by targeting the hERG channel. Eur J Pharmacol. 2021;893: 173813. doi:10.1016/j.ejphar.2020.173813

47. Gutenkunst RN, Waterfall JJ, Casey FP, Brown KS, Myers CR, Sethna JP. Universally Sloppy Parameter Sensitivities in Systems Biology Models. PLoS Comput Biol. 2007;3: e189. doi:10.1371/journal.pcbi.0030189

48. Brown KS, Hill CC, Calero GA, Myers CR, Lee KH, Sethna JP, et al. The statistical mechanics of complex signaling networks: nerve growth factor signaling. Phys Biol. 2004;1: 184. doi:10.1088/1478-3967/1/3/006

49. Casey FP, Baird D, Feng Q, Gutenkunst RN, Waterfall JJ, Myers CR, et al. Optimal experimental design in an epidermal growth factor receptor signalling and down-regulation model. IET Syst Biol. 2007;1: 190–202. doi:10.1049/iet-syb:20060065

50. Forny C, Sube R, Ertel EA. Contractions of Human-iPSC-derived Cardiomyocyte Syncytia Measured with a Ca-sensitive Fluorescent Dye in Temperature-controlled 384-well Plates. J Vis Exp JoVE. 2018; 58290. doi:10.3791/58290

51. Lian X, Hsiao C, Wilson G, Zhu K, Hazeltine LB, Azarin SM, et al. Robust cardiomyocyte differentiation from human pluripotent stem cells via temporal modulation of canonical Wnt signaling. Proc Natl Acad Sci U S A. 2012;109: E1848–E1857. doi:10.1073/pnas.1200250109

52. Greenberg MJ, Daily NJ, Wang A, Conway MK, Wakatsuki T. Genetic and Tissue Engineering Approaches to Modeling the Mechanics of Human Heart Failure for Drug Discovery. Front Cardiovasc Med. 2018;5. Available: https://www.frontiersin.org/articles/10.3389/fcvm.2018.00120